Advantage of Being a Dimer for *Serratia marcescens* Endonuclease

Chuanying Chen,[†] Kurt Krause,[‡] and B. Montgomery Pettitt*[,†,§]

Department of Chemistry, University of Houston, Houston, Texas 77204-5003, Department of Biology and Biochemistry, University of Houston, Houston, Texas 77204-5001, and Department of Biochemistry, University of Otago, Dunedin, New Zealand 9001

Received: July 1, 2008; Revised Manuscript Received: October 3, 2008

The monomer and dimer of the bacterium *Serratia marcescens* endonuclease (SMnase) are each catalytically active, and the two subunits of the dimer function independently of each other. Nature, however, chooses the dimer form instead of the monomer. In order to explain this, we performed molecular dynamics (MD) simulations of both model-built complexes of a subunit of SMnase and the dimer with DNA in aqueous solution. We estimated the electrostatic binding energy, analyzed the distribution and dynamics of water around the complexes, identified water clusters in the protein, and related the dynamics of water to the protein's function. We find that the dimer form has an electrostatic advantage over the monomer to associate with DNA. Although Mg^{2+} remains hexa-coordinated during the simulation, the binding pathway of DNA to Mg^{2+} changes from inner-sphere binding in the monomer to outer-sphere in the dimer, which may be more energetically favorable. In addition, two water clusters in the active site of each monomer and in the dimer complex were identified and localized in two regions, named the "stabilizing" and "working" regions. Water in the "working" region in the dimer complex has larger fluctuations than that in the monomer.

Introduction

Enzymes in the family of sugar-nonspecific endonucleases have been isolated from a wide range of sources from bacteria to mammals.[1] They can be characterized by their abilities to hydrolyze both DNA and RNA. Although these enzymes have been extensively studied in terms of their catalytic properties and biological roles, the relationship between structure and function is still unclear. So far, only a few enzymes have been crystallized, including *Staphylococcal* nuclease,[2] *Serratia marcescens* nuclease,[3,4] P1 nuclease from *Penicillium citrinum*,[5] Vvn from *Vibrio vulnificus*,[6] and the nuclease domain of ColE7[7] and ColE9[8] from *E. coli*. Among them, only Vvn[6] and the nuclease domain of ColE7[9] and ColE9[10] have been solved with a dsDNA substrate. Of all of these sugar-nonspecific endonucleases, *Serratia marcescens* endonuclease (SMnase) is the most studied one because of its broad class of substrates, very high specific activity, and wide commercial applications. Here, we present a study of the structure−function relationship of the cleaving mechanism and hope this study might help us understand the evolutionary aspects of this family.

SMnase is a homodimer, each with 245 amino acids (Figure 1). It is capable of cleaving single- and double-stranded DNA and RNA with a slight preference to A-form nucleic acids.[11,12] In the presence of magnesium, it produces 5′-phosphorylated and 3′-OH oligonucleotides. Since there is no structural data available for the enzyme−substrate complex, it has been of difficulty to verify the precise catalytic mechanism for SMnase. However, after comparing the three-dimensional structure of the complex of I-PpoI and its cognate substrate with SMnase, a similar motif at both active sites has been identified. The motif, a $\beta\beta\alpha$-Me finger, composed of two beta-strands, a helix, and a metal, makes a common core of the active site for endonuclease activity.[3,15] Mutational and structural analysis propose for SMnase, Arg57, His89, Asn119, and Glu127 to play a central role in the catalytic process.[13,14] During this process, oxygen atoms from the phosphate group of DNA bind to Mg^{2+} directly. His89 acts as a general base to activate the water molecule for a nucleophilic attack on the phosphorus atom, while Arg57 stabilizes the transition state and the leaving group as well.[16]

One interesting feature of SMnase is that the protein functions as a dimer in nature. Experiments show that both the monomer and dimer can function with the same specific activity, and each subunit of the protein cleaves the substrate independently.[17] This does not mean that the favored dimeric state of SMnase exists without any advantage for *Serratia marcescens*. Kinetic studies of a series of monomer variants and the dimer[18] showed that the time course of the reaction is different between the monomer and dimer. Under the conditions of low enzyme concentration and high molecular weight DNA substrate, the dimer functions in a processive manner. This might be more effective than a monomer following a distributive mechanism, because the rate limiting step of the reaction is either the association of the protein with the substrate or the cleavage of the substrate. Nevertheless, how the monomer and dimer work in such a different manner has not been well addressed.

Our previous studies of the hydration patterns of the monomer, the dimer, and one model-built complex of the monomer with its DNA substrate demonstrated that the interior hydration sites identified in the averaged configuration over molecular dynamics (MD) snapshots have ∼88% similarity with crystal water molecules.[19,20] Even though the general hydration pattern of the protein does not change very much on dimerization outside of the direct interface, the local dynamics of water may be affected, particularly at the active site. This might consequently influence the mechanism of the cleavage of DNA. However, whether dimerization has an effect on the association of DNA is still in question.

[†] Department of Chemistry, University of Houston.
[‡] University of Otago.
[§] Department of Biology and Biochemistry, University of Houston.

10.1021/jp8057838 CCC: $40.75
Published on Web 11/20/2008

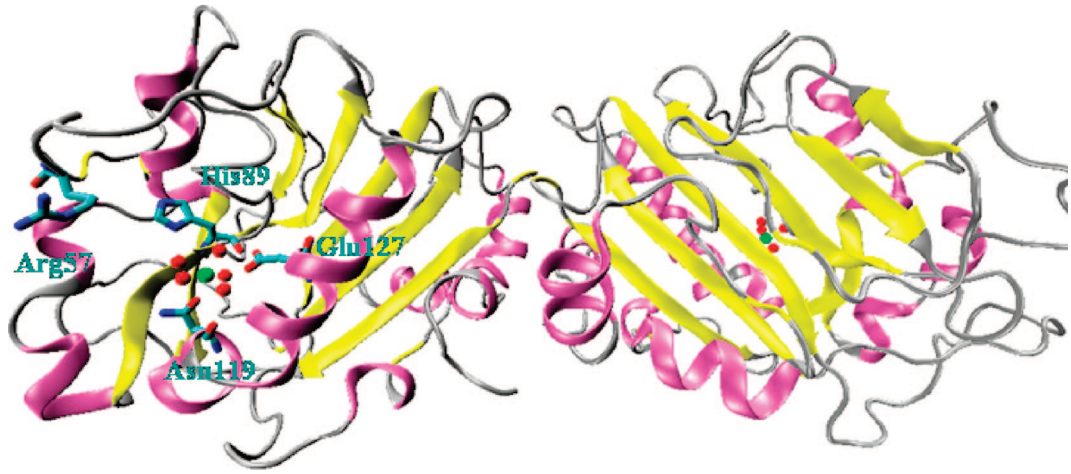

Figure 1. Homodimer structure of *Serratia marcescens* endonuclease (SMnase). Mg^{2+}, green sphere; water molecules coordinating to Mg^{2+}, red spheres. Arg57, His89, Asn119, and Glu127 are also shown.

Nonspecific proteins binding to DNA differ from specific ones generally in that (i) association between the partners is mainly driven by electrostatic interactions with lower affinity and stronger dependence of ionic strength, (ii) the interface of protein and DNA are thought to be more hydrated, and (iii) both protein and DNA have less conformational change.[21,22] As such, it is reasonable to evaluate the binding free energy assuming that the conformations of the protein and DNA taken from the complex trajectory are comparable to the free forms. In addition, we approximate the binding free energy by only considering the electrostatic contribution.

In this work, MD simulations of model-built monomer−DNA and dimer−DNA complexes have been carried out to further understand the effects of dimerization on the catalytic process of SMnase, such as DNA association, cleavage, transition-state stabilization, leaving group protonation, and DNA dissociation. By comparing the monomer−DNA with dimer−DNA complex conformers via the electrostatic contributions to the binding energy as well as in the hydration patterns, especially at the protein−DNA interface and the active site, we are able to propose a mechanism for the advantages of being a dimer for SMnase over a monomer.

Methods

MD Simulation. Due to the lack of structural data for SMnase with its substrate, the protein−DNA complex system was built by superimposing the structure of I-PpoI endonuclease (PDB code 1A73) on the subunit B of SMnase (PDB code 1QAE) using CHARMM,[23] based on the structural similarity at the active site of I-PpoI endonuclease and SMnase.[16] It has been shown that SMnase has a slight preference for A-form DNA such as in $d(GGGGCGCCC)_2$. Therefore, a 16-mer DNA duplex, $d(ATAGGGGCGCCCCTAT)_2$, was first constructed in ideal A-form and then "threaded" through the backbone of the I-PpoI DNA. The details of the construction of the protein−DNA complex model were described elsewhere.[19] Protein residues 1−5, not given by the diffraction results, were also built. As for the monomer−DNA complex, the monomer was taken from the subunit B of the dimer. We used independent runs of the monomer and dimer rather than just averaging the two monomers from a dimer run so as not to bias the symmetry and outcome.

The systems were simulated using the program ESP[24] and the all-atom CHARMM 27 parameter set.[25,26] Equations of motion were integrated with a 2 fs time step in the microcanonical ensemble (NVE) with periodic boundary conditions. Electrostatic interactions were treated with an Ewald sum[27] using a fast linked-cell algorithm. The complexes were put into pre-equilibrated boxes of water using standard setup procedures (See ref 19). The system setup of the monomer−DNA and dimer−DNA is summarized in Table 1. After several steepest descent energy minimization steps, the system was equilibrated at 300 K for 3.0 ns (monomer−DNA) and 6.9 ns (dimer−DNA) until geometries and energies for the complexes were stable. The trajectory was then continued to 11.1 ns for the monomer−DNA and 12.9 ns for the dimer−DNA, and coordinates were saved for analysis at an interval of 0.1 ps.

TABLE 1: System Setup of the Monomer and Dimer Complex Systems

	monomer−DNA	dimer−DNA
box size (Å)	86.65 × 87.68 × 65.89	130.55 × 129.68 × 129.51
no. solute atoms	4730	8448
no. TIP3P waters	15 324	70 896
no. Na^+	55	80
no. Cl^-	25	50

Analysis of Contacts. In general, protein and DNA are held together by electrostatic, hydrophobic, direct hydrogen bond (H-bond), and water-mediated interactions. Herein, a strong salt-bridge contact was defined between a pair of charged nonhydrogen atoms when the distance was less than 2.8 Å, and a hydrophobic interaction was defined when the distance between a pair of low charged carbon atoms (e.g., not carbonyl) was less than 4.0 Å. A hydrogen bond interaction in a donor−acceptor pair, A···H-D, satisfied a set of specified geometrical criterion, in which they are described as the following: (i) that the distance between H (hydrogen) and A (acceptor) should be smaller than 2.3 Å, (ii) that the distance between A and D (donor) should be smaller than 3.2 Å, and (iii) that the angle between A, H, and D should be between 130 and 180°. A water-mediated hydrogen bond interaction was claimed when a hydration site occupied by water molecules was in proximity to either other waters or protein/DNA.

Electrostatic Binding Energy Calculations. The total electrostatic binding energy of a protein and DNA molecule can be expressed by

$$\Delta\Delta G_{ele} = \Delta G_{ele}(\text{complex}) - \Delta G_{ele}(\text{protein}) - \Delta G_{ele}(\text{DNA}) \quad (1)$$

where ΔG_{ele} is the electrostatic potential of the molecule or complex. The electrostatic potential of a macromolecule system in a monovalent salt solution may be roughly approximated using the Poisson−Boltzmann (PB) equation.[28] On the basis of the thermodynamics, the total electrostatic potential can be decomposed into salt-independent ΔG_{ns} and salt-dependent ΔG_s parts.[29] The salt-independent potential is composed of two terms:

$$\Delta G_{ns} = \Delta G_{coul} + \Delta G_{hyd} \quad (2)$$

where ΔG_{coul} is the Coulombic interaction in the solute's dielectric medium ε_m and ΔG_{hyd} is the hydration energy in the heterogeneous environment, in which the solute has an interior dielectric constant of ε_m and the solvent has ε_s. In the presence of mobile ions, the sum of ΔG_{hyd} and ΔG_s gives the electrostatic solvation energy. If it is assumed the electrostatic part of the binding free energy entirely dominates the reaction, then the salt-dependent contribution to the total electrostatic energy should change linearly with the logarithm of salt concentration M^+

$$-\frac{\partial \ln[K_{obs}]}{\partial \ln[M^+]} = \frac{1}{RT}\frac{\partial \Delta\Delta G_s^0}{\partial \ln[M^+]} \quad (3)$$

where K_{obs} corresponds to the observed association constant, $[M^+]$ represents the monovalent salt concentration, R is the gas constant, T is the absolute temperature, and $\Delta\Delta G_s$ is the change in salt-dependent contribution to the electrostatic binding energy.

In calculation of the structurally averaged electrostatic binding energy, the coordinates of structures were extracted every 500 ps from the trajectories. The APBS package[30] was used for all of the PB calculations with the CHARMM 27 parameter set[25,26] for atom charges and radii. The dielectric constant of DNA and protein was set to 4, and the solvent, to 78. An ionic strength of 0.1 M was used with the radius of the monovalent ion exclusion region set to 2 Å. A dielectric boundary spline was used with a window size of 0.3 Å to reduce the grid sensitivity.[31] All calculations were started with grid size at 0.6 Å and then focused to a final grid spacing of 0.4 Å. Approximately 1% difference in electrostatic binding energy was found when the higher resolution was used.

Hydration Properties of the Complex. Hydration properties include localization of the hydration sites, evaluation of water residence time, and the dynamics of hydrogen bond interactions of water−water and water−protein at the hydration sites. Hydration sites may be defined as any local maximum in the water (oxygen) density map that satisfies certain protein proximity conditions. Obtaining the average solvent density map and localizing the hydration sites from an MD trajectory has been described in detail elsewhere.[19,32] Briefly, hydration sites were obtained using a grid spacing of 0.5 Å, a number density threshold of 1.5 per grid point, and a minimum distance of 2.8 Å which separates neighboring sites.

The dynamics of water at a hydration site can be described by water molecule residence time and lifetime of H-bond interactions which can be for water−water and water−protein/DNA residues. Water residence times can indicate how water around the protein differs from the bulk. The fluctuations of hydrogen bonds within water as well as between water and the macromolecule contribute to the mechanistic description in terms of how the dynamics of water is related to the protein's function.

The water residence time at a hydration site was evaluated from an occupation survival time correlation function $C_\alpha(t)$ that represents the average number of water molecules that remain in the hydration site for a duration of time.[32] The occupation survival function is defined as

$$C_\alpha(t) = \sum_{j=1}^{N_w} \frac{1}{T_{run} - t + 1} \sum_{t_0}^{T_{run}-t} p_{\alpha,j}(t_0, t_0 + t) \quad (4)$$

where $p_{\alpha,j}(t_0,t_0+t)$ is a binary function that takes the value of 1 if the jth water molecule has occupied the αth site from t_0 to t_0+t; otherwise, the function is 0. Also in here, N_w is the total number of water molecules and T_{run} is the length of the simulation. Previous work[20] from the survival function for the hydration sites around the active site indicated that most sites were not well fit by a single exponential. We found the relaxation time behavior is better approximated with two terms using a stretched exponential for the long time decay (a Kohlraush−Williams−Watts model[33]), and a single exponential for the short time decay

$$C_\alpha(t) = W_0\{(1 - x)\exp[-t/\tau_f] + x\exp[-(t/\tau_s)^\beta]\} \quad (5)$$

where W_0 is the occupancy of the αth site, τ_f and τ_s are the fast and slow residence times, respectively, x is the weight of the slow relaxation, and β is a stretching parameter between 0 and 1, which reflects the extent to which the relaxation process deviates from exponential behavior and provides us additional information upon the heterogeneity of the water dynamics around the molecule. Such nonexponential behavior has commonly been found in both amorphous and glassy condensed phase systems as well.[34,35]

The dynamics of hydrogen bond interactions of water−water and water−protein/DNA at the hydration sites was investigated by calculating the average lifetime of the hydrogen bonds. The decay was evaluated by calculation of a hydrogen bond lifetime correlation function[36,37]

$$S_\alpha(t) = \frac{\langle h(t_0)\, H(t_0 + t)\, p_\alpha(t_0)\rangle}{\langle h\rangle} \quad (6)$$

where function $p_\alpha(t_0)$ is unity when a particular water molecule occupies the αth hydration site at original time t_0 and otherwise it is 0; $h(t)$ is a hydrogen bond indicator, which is unity when the water molecules inside the αth hydration site forms a pair with another molecule by hydrogen bonding at time t, and otherwise it is 0; $H(t_0+t)$ is 1 if the tagged pair remains continuously hydrogen bonded during time $t_0 + t$ and otherwise it is 0; and $\langle ... \rangle$ denotes an average over all hydrogen bonds that are present at t_0 for the αth site. With this construct, $S_\alpha(t)$ describes the probability that a water pair, which occupies the αth hydration site, is continuously hydrogen bonded from time t_0 to t. Similar to water residence times at the hydration sites, the decay of $S_\alpha(t)$ around the active site is also expected to obey a KWW model.

Results and Discussion

Protein−DNA Contacts. Protein and DNA molecules generally utilize their chemical and geometrical properties to facilitate their recognition and association. The protein and DNA are held together by a mix of salt-bridges, water-mediated and direct

TABLE 2: Primary Contacts between Protein and DNA (Only Contacts with Frequencies Larger than 0.10 Are Shown)

	monomer−DNA			dimer−DNA		
	H-bond	salt-bridge	water-med.	H-bond	salt-bridge	water-med.
Mg^{2+}		1.00 (G25,O2P)				0.90 (C24,O3S)
Ser53				0.43 (G23,O2P)		
Thr56	0.82 (A3,O1P)			0.62 (G4,O1P)		
Arg57	0.46 (C27,O1P)	0.15 (C27,O1P)	0.10 (C27,O1P)	0.96 (C26,O1P)	0.66 (C26,O1P)	0.31 (C26,O1P)
Asn58	0.39 (A3,O1P)			0.45 (G4,O1P)		0.20 (G4,O1P)
Lys60				0.33 (A3,O2P)		
Asn80			0.15 (C26,O2P)	0.79 (C26,O2P)		
Asp86			0.48 (C26,O2P), 0.22 (G25,O3S)			
Arg87	0.21 (C27,O1P)	0.15 (C27,O1P)	0.25 (C26,O1P)	0.65 (C26,O2P)	0.20 (C26,O2P)	0.58 (G25,O2P)
His89			0.22 (C26,O1P)			0.19 (G25,O2P)
Gln120	0.44 (G9,H22)					
Arg125	0.86 (C11,O3S), 0.90 (C12,O2P)	0.64 (C12,O2P)		0.15 (C13,O2P)	0.22 (C13,O2P)	
Asp128			0.20 (C24,O2P)			0.25 (C12,O3S)
Lys196	0.37 (C10,O4S)			0.68 (C11,O2P)	0.53 (C11,O2P)	
Asp199			0.15 (C12,O2P)			

hydrogen bond interactions between the protein and DNA backbone, as summarized in Table 2. That almost no DNA bases are directly involved in the contacts is consistent with the reduced specificity of the enzyme in recognition of its substrate. However, these DNA contacts slightly reorganize from the monomer to dimer simulations, as shown in Figure 2A and B. Particularly, in the monomer, one nonbridging oxygen atom from Gua25 directly binds to Mg^{2+} with 100% strength. Arg57 interacts with Cyt27 with a frequency of 0.15 by salt-bridge, 0.55 by direct H-bond, and 0.10 by water-mediated hydrogen bond. While in the dimer, DNA binds to Mg^{2+} indirectly with a frequency of 0.90 between one bridging oxygen atom 3′-O of Cyt24 and a water molecule coordinating to Mg^{2+}. Arg57 interacts with Cyt26 with a frequency of 0.66 by salt-bridge, 0.96 by direct H-bond, and 0.31 by water-mediated H-bond, much more strongly than those happening in the monomer.

Previous studies of the free protein systems[14,20] showed that Mg^{2+} has an octahedral coordination with five water molecules and OD1 from the side chain of Asn119. The distance between Mg^{2+} and each oxygen atom of the ligands is 1.97 ± 0.06 Å on average during the entire simulation, close to the value in the crystal structure which is in the range between 2.01 and 2.13 Å.[4] However, in the complex systems, although Mg^{2+} maintains a hexa-coordinated structure, ligand exchange for Mg^{2+} occurs on the simulation time scale (Figure 3A for the monomer−DNA and Figure 3B for the dimer−DNA). For the monomer, upon DNA binding to the protein, the contact of Asn119 with Mg^{2+} takes place by one carboxylic oxygen atom, OE1 from Glu127. The distance between OE1 and Mg^{2+} is shortened to 1.87 ± 0.05 Å. The other carboxylic oxygen, OE2 from Glu127, and one nonbridging oxygen atom, O2P from Gua25 of DNA, substitute two water molecules for inner-sphere

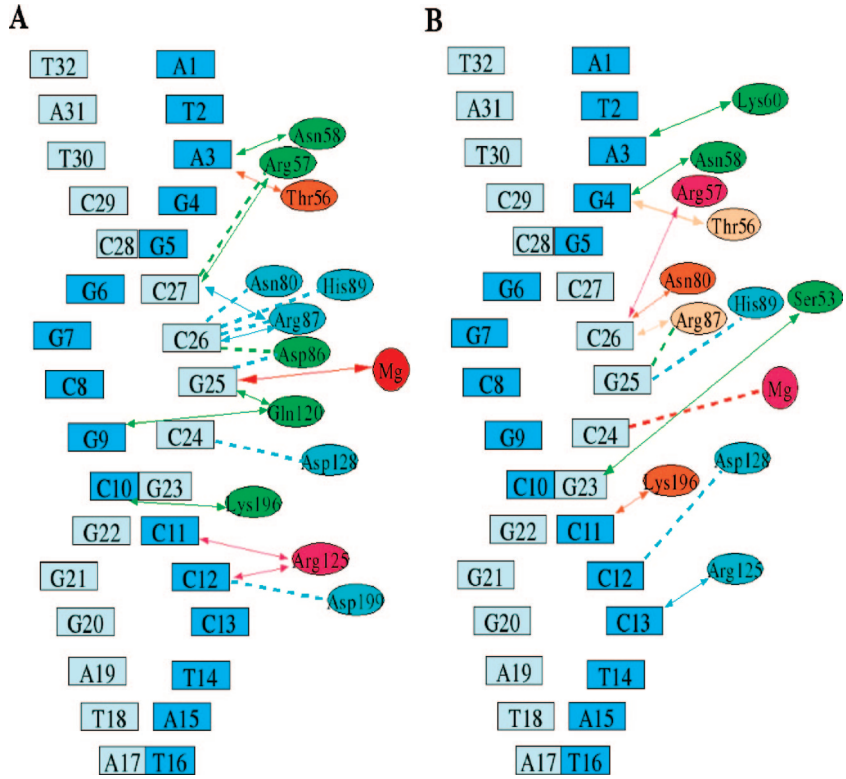

Figure 2. Diagram of primary contacts between protein and DNA: (A) monomer−DNA complex; (B) dimer−DNA complex. ↔, direct contacts; - - -, water-mediated contacts. The contact strengths in different levels of color are red (100%), light red (>90%), orange (>70%), pink (>50%), green (>30%), and cyan (>10%).

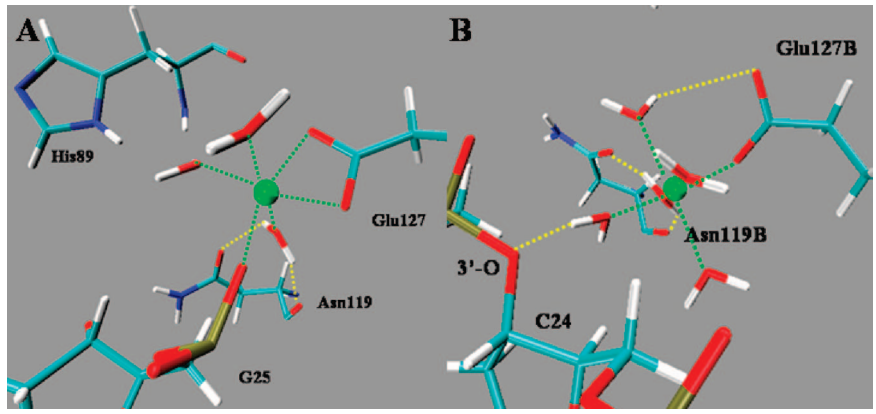

Figure 3. Mg^{2+} coordinations at the active site: (A) monomer−DNA complex; (B) dimer−DNA complex. Mg^{2+}, green sphere.

coordination to Mg^{2+}, giving a distance of 1.90 ± 0.06 and 1.84 ± 0.04 Å, respectively. As for the dimer, DNA takes a different binding mode to Mg^{2+}. Substitution involving Asn119B is the same as in the monomer, but five water molecules remain unchanged. One bridging oxygen atom, 3′-O from Cyt24, binds to Mg^{2+} via one ligand water with more than 90% frequency. As a result, DNA binding to Mg^{2+} changes from the inner sphere in the monomer to the outer sphere in the dimer.

SMnase is a sugar-nonspecific endonuclease with only slight sequence specificity, whereas I-Ppol is a highly sequence-specific homing endonuclease. Although the similar motif at their active sites suggests a similar cleaving action, it does not require that the same binding mode to the substrate should obtain. Therefore, it is necessary to investigate the association of the protein with DNA both structurally and energetically. Structurally, new models based on the sugar-nonspecific endonuclease−DNA complex are required. Although it is difficult to cocrystallize such protein with its substrate because of the weaker binding affinity and less ordered association, the sugar-nonspecific endonuclease of Vvn (*Vibrio vulnificus)* with its short 8-base-pair DNA substrate has been refined (PDB code 1OUP).[6] Around their active sites, superposing residues 85−89 and 111−123 from SMnase on residues 76−80 and 119−131 from the Vvn−DNA complex gives a backbone root-mean-square deviation (rmsd) of 1.2 Å. In the procedure of building new models on Vvn, water molecules coordinated to Mg^{2+} in the crystal structure were either kept or removed. Therefore, for both the monomer and dimer state, four new complex models were built. As described in the Methods section, the same simulation procedure was performed on these four models. It was found that, after the equilibration phase, unlike the models built on I-Ppol, Asn119 remains coordinated to Mg^{2+} in all four models. However, regardless of whether Mg^{2+} is unhydrated or hydrated in its initial structure, the monomer models have the same inner-sphere binding mode, while the dimer models have the same outer-sphere binding mode, as observed above.

It is well-known that magnesium plays a central role as a metal cofactor in nucleic acid biochemistry. Mg^{2+} possesses special properties, including small size, high charge density, and extensive hydrated state, which distinguish it from other alkali and alkaline earth metals, such as Na^+, K^+, and Ca^{2+} [38] in biological activity. In the current potential energy function (PEF), interactions between Mg^{2+} and its ligands are often described by electrostatic and van der Waals (vdW) forces with appropriate vdW parameters. A full +2e charge is constant for Mg^{2+}. This model allows the flexible movements of ligands at the metal-binding site. Although the current PEF does not explicitly include charge transfer and local polarization effects, it is plausible because Mg^{2+}, being a hard cation, is less polarizable than soft cations and interacts mainly electrostatically with its ligands. Thus, the use of a mean field model of polarizability in this case is not obviously unreasonable.

The MD simulations of the free SMnase systems[20] reproduced the experimentally observed metal coordination number and structural geometry of the Mg−ligand cluster.[14] Theoretical studies of hydration properties of Mg^{2+} [39,40] showed that in water it takes 18.4 kcal/mol to remove one water molecule from a hexa-hydrated Mg^{2+}. For a penta-hydrated Mg^{2+}, 27.4 kcal/mol of energy is needed for the dehydration to form a tetra-hydrated Mg^{2+}. If more water molecules are removed, the corresponding dehydration energy increases. As a consequence, in the case of SMnase, in the monomer, the hydrated Mg^{2+} has to partially exchange its one- or two-coordinated water molecules in order to coordinate with DNA or OE2 of Glu127, which appears to be energetically costly. In addition, both experimental and theoretical studies[38,41,42] supported the propensity of magnesium to interact with oligonucleotides in an outer-sphere mode. Considering that association of the substrate to the protein is rate limiting, it is reasonable to hypothesize that the favorable binding energy of DNA to Mg^{2+} in the dimer might be one advantage of dimerization of SMnase.

Electrostatic Contributions to the Binding Energy. As shown in Figure 4, the electrostatic surface potentials from the proteins and DNA are very complementary. On the face of the active site (Figure 4A for the dimer and Figure 4B for the monomer), a strong positively electrostatic field attracts the DNA molecule, whereas, on the opposite side of the active site (Figure 4C for the monomer) or in the region of the dimeric interface (Figure 4A), the strong negative field repels DNA and orients it toward the active site for binding.[3]

Table 3 presents contributions to the electrostatic binding energy estimated with the Poisson−Boltzmann equation with ionic strengths of 0 and 0.1 M, respectively. Overall, the long-range Coulombic energy dominates the electrostatic binding. With $\varepsilon_m = 4$, the salt-independent component $\Delta\Delta G_{ns}$ favors the binding for both the monomer and dimer, but the salt-dependent component $\Delta\Delta G_s$ compensates in the opposite direction. The dimer state has a more negative $\Delta\Delta G_{ns}$, −60.0 ± 5.9 kJ/mol, than that of the monomer, −48.8 ± 7.6 kJ/mol. In addition, the dimer state has a less positive $\Delta\Delta G_s$ value of 25.3 ± 4.4 kJ/mol than 39.4 ± 3.5 kJ/mol found for the monomer. Therefore, in terms of the electrostatic binding energy, the dimer appears to associate more favorably with DNA than the monomer. As the net charge of the monomer as modeled here is zero, dimerization does not increase the net charge of the system. As a consequence, the total electrostatic binding

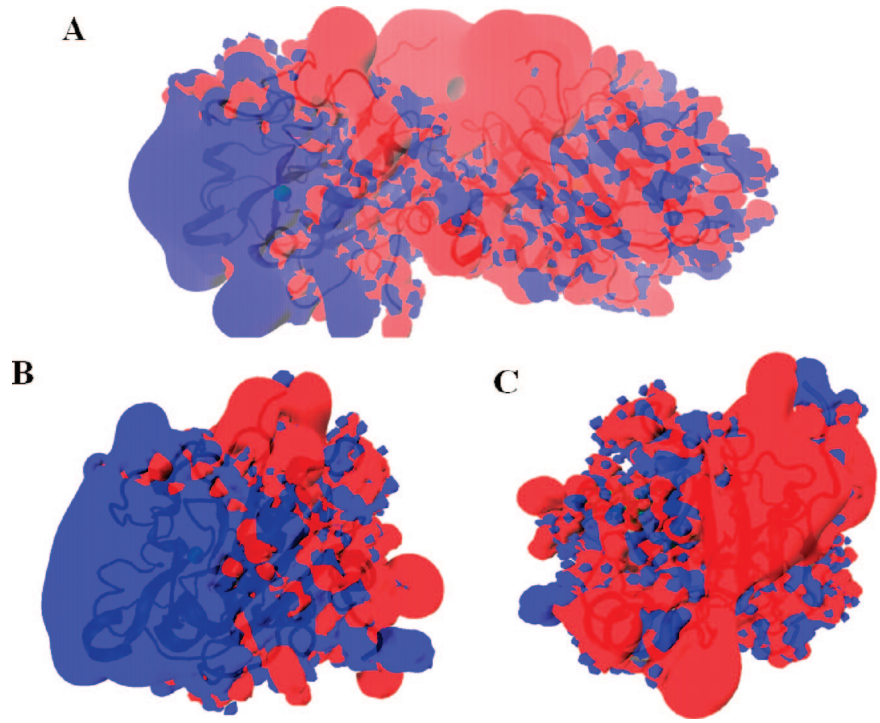

Figure 4. ±2 kT/e electrostatic potential isocontours of SMnase (blue, +; red, −) in a monovalent salt of 0.1 M concentration: (A) in the face of the active site of the subunit B from the dimer; (B) in the face of the active site of the monomer; (C) on the opposite side of the active site of the monomer.

TABLE 3: Contributions to the Calculated Electrostatic Binding Energy of the SMnase−DNA Complex at a Salt Concentration of 0.1 M with ε_m at 4, 8, and 20 (Energy in kJ/mol)

	monomer−DNA	dimer−DNA
	$\varepsilon_m = 4.0$	
$\langle\Delta\Delta G_{coul}\rangle$	−1642.5 ± 110.7	−1453.0 ± 77.2
$\langle\Delta\Delta G_{hyd}\rangle$	1592.7 ± 104.6	1392.5 ± 74.5
$\langle\Delta\Delta G_{ns}\rangle$	−48.8 ± 7.6	−60.0 ± 5.9
$\langle\Delta\Delta G_{s}\rangle$	39.4 ± 3.5	25.3 ± 4.4
$\langle\Delta\Delta G_{ele}\rangle$	−9.4 ± 6.0	−34.7 ± 3.7
	$\varepsilon_m = 8.0$	
$\langle\Delta\Delta G_{coul}\rangle$	−821.2 ± 55.3	−727.5 ± 40.1
$\langle\Delta\Delta G_{hyd}\rangle$	753.1 ± 49.1	660.9 ± 36.0
$\langle\Delta\Delta G_{ns}\rangle$	−67.6 ± 6.7	−66.3 ± 5.5
$\langle\Delta\Delta G_{s}\rangle$	40.2 ± 3.2	26.5 ± 4.2
$\langle\Delta\Delta G_{ele}\rangle$	−28.3 ± 4.1	−39.8 ± 2.6
	$\varepsilon_m = 20.0$	
$\langle\Delta\Delta G_{coul}\rangle$	−328.5 ± 22.1	−290.6 ± 15.4
$\langle\Delta\Delta G_{hyd}\rangle$	249.5 ± 15.9	220.2 ± 11.1
$\langle\Delta\Delta G_{ns}\rangle$	−78.8 ± 6.4	−70.3 ± 4.8
$\langle\Delta\Delta G_{s}\rangle$	41.5 ± 2.7	27.1 ± 6.3
$\langle\Delta\Delta G_{ele}\rangle$	−37.3 ± 4.1	−43.2 ± 5.7

energy is affected by the distance between the partners and/or the charge distribution within the protein.

The exact binding value calculated from the PB method strongly depends on the parameters used in the calculations, especially the solute−solvent boundary and the interior dielectric constant. A uniform dielectric constant of 2 or 4 for the solute is routinely used to account for the effect of electronic polarizability or small dipolar fluctuations that may accompany structural transitions in proteins.[43] However, with the solvent surface definition, these values are found to overestimate the desolvation cost of charges and the strengths of charge−charge interactions when pK_a values are predicted. Antosiewicz et al.[44] proposed using a higher value of $\varepsilon_m = 20$, which effectively produces better agreements with the experimental pK_a's. Dong et al.[51] studied the contributions of electrostatic interactions to the binding stability of barnase and barstar using three protocols to define the dielectric boundary and ε_m. They found that the vdW surface with $\varepsilon_m = 4$ is most consistent with the experiment. The solvent exclusion (SE) surface with $\varepsilon_m = 20$ is qualitatively similar to the vdW surface with $\varepsilon_m = 4$. In contrast, the SE surface with $\varepsilon_m = 4$ destabilizes the binding. Although their studies do not consider the structural relaxation and sampling of protein conformation, their conclusion is a caveat to the electrostatic contribution sensitivity to a particular PB protocol.

In the past two decades, considerable theoretical work has been done to estimate ε_m. Making use of the extended Fröhlich−Kirkwood theory of solute dielectric properties, van Gunsteren and his co-workers[52,53] showed that the static dielectric constants of proteins are in the range between 17 and 40 at 300 K. ε_m is about 2−4 in the protein core but increases when one extends to the protein surface where the charged groups most frequently occur. Therefore, charged surface residues are the dominating components of the higher dielectric permittivity estimates. Yang et al.[54] studied a system of a DNA molecule in the salt solution and found that the phosphate parts are the primary determinant of the overall DNA dielectric constant which is ∼16. In addition, the dielectric constant of water in that high salt system was ∼41, smaller than 71 for pure SPC/E water[55] in part due to the well-known saline dielectric decrement.[56] It appears the dielectric constant of a solute is somewhat system-dependent. A lack of universality for ε_m presents a challenge for continuum methods.

In the case of SMnase, Antosiewicz et al.[45] found that pK_a values of His89, Asp86, and Asp128 are increased by 1 upon DNA binding for both the monomer and dimer state. In the current MD simulations and studies, the ionized state of the residues is not considered, and a uniform dielectric constant for the solute is used in the PB calculations with the nonoptimized atomic radii for the dielectric spline-based boundary. The

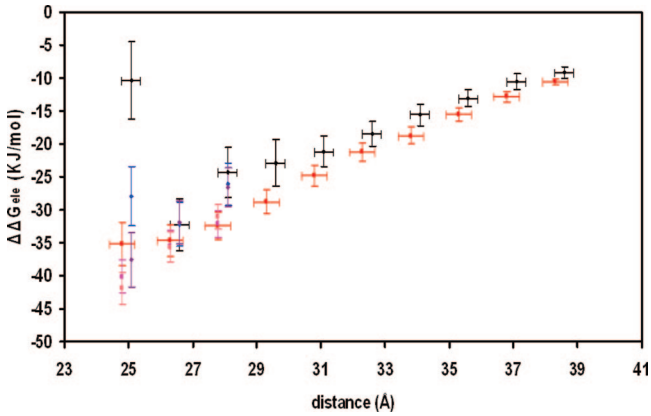

Figure 5. Calculated total electrostatic binding energy versus distance between the protein and DNA in 0.1 M salt solution with $\varepsilon_m = 4$. $\Delta\Delta G_{ele}$ and distance are averaged over the set of the snapshots from the trajectory. Distance is defined between the center of DNA and the center of the monomer or subunit B of the dimer. For the monomer, with $\varepsilon_m = 4$, black; $\varepsilon_m = 8$, blue; $\varepsilon_m = 20$, purple. For the dimer, with $\varepsilon_m = 4$, red; $\varepsilon_m = 8$, magenta; $\varepsilon_m = 20$, pink.

current work is not designed to define better PB parameters for the complex system but to compare two protein states with reasonable parameter sets and under the same conditions. Because the interface of the protein and DNA is full of charged side chains, such as Arg57, Arg87, Arg125, Arg196, and Mg^{2+}, it is reasonable to increase the dielectric constant to higher values in the range 8−20 for comparison. In 0.1 M salt, higher dielectric constants of 8 and 20 reduce $\Delta\Delta G_{ele,mp}$ of the monomer state markedly by 19 and 28 kJ/mol, respectively, while for the dimer, by only about 5 and 8 kJ/mol in both cases. One possible reason explaining these differences is the direct binding of DNA to Mg^{2+} in the monomer.

When the monomer is moved away from the DNA along the direction of the center of each molecule by 1.5 Å, $\Delta\Delta G_{ele,mp}$ (in black) becomes more negative and relatively close to $\Delta\Delta G_{ele,dp}$ for the dimer (in red), shown in Figure 5. As for the dimer state, moving the protein away from the DNA by 1.5 Å does not influence the total electrostatic binding energy very much. When the distance between the DNA and the protein is longer than 1.5 Å, having the higher ε_m value with 8 or 20 has little effect on the electrostatic binding energy for either state. As expected, the total electrostatic binding energy increases when the distance becomes longer. It seems that this configuration of the monomer and DNA with the distance at 1.5 Å is the most favorable one when comparing other configurations at a longer distance. Indirect binding to Mg^{2+} appears to be favorable.

As for the salt-dependent electrostatic binding energy, the monomer and dimer have $\Delta\Delta G_s$ values of 39.4 ± 3.5 and 25.3 ± 4.4 kJ/mol, respectively, in the 0.1 M salt. Overall, $\Delta\Delta G_s$ destabilizes the protein−DNA complex, and it is independent of the protein's dielectric constant. In order to estimate the dependence of the electrostatic binding energy on the salt concentration, the electrostatic binding energy was calculated for the monomer and dimer states in the range of the monovalent salt from 0.05 to 0.4 M, and the plot of $\Delta\Delta G_s/RT$ versus $\log[M^+]$ is shown in Figure 6. As expected, $\Delta\Delta G_s$ increases linearly with the salt concentration. According to the studies by Record et al.,[46] the salt dependence of association follows $-\partial(\ln K_{obs})/\partial(\ln[M^+]) = m'\psi$, where m' is the number of ion pairs formed with DNA and ψ is the fraction of counterions bound to each DNA phosphate. $\psi = 0.88$ for double-stranded DNA, while $\psi = 0.64$ when short double-stranded DNA is considered.[47] For

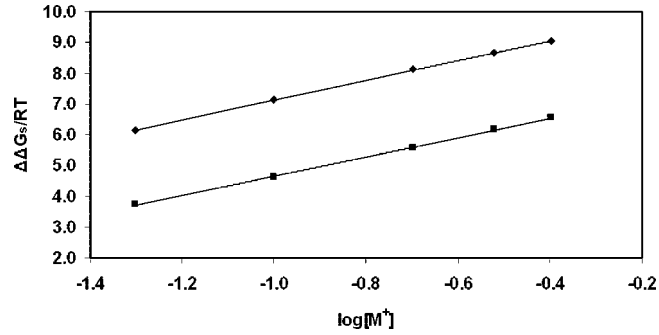

Figure 6. Calculated salt dependence of the electrostatic binding energy of SMnase in a monovalent salt solution with $\varepsilon_m = 4$: (◆) monomer−DNA complex; (■) dimer−DNA complex.

the sequence-nonspecific binding proteins with DNA, experiments give $m'\psi$ of about 4−7 if $\psi = 0.64$.[22] In the case of SMnase, the slope of the fitted line of $\Delta\Delta G_s/RT$ versus $\log[M^+]$ is about 3.2 ± 0.3, the same for both the monomer and the dimer. The calculated $m'\psi$ is in reasonable agreement with the experimental data[22] on other systems.

The kinetic studies found that the rate limiting step of the reaction is the association of the protein and DNA or the cleavage of DNA.[18] When the association is rate limiting, the experimental finding[18] that the dimeric form cleaves the DNA substrate more processively than the monomer can be explained by the estimated electrostatic binding energy. In the processive manner, the dimer stays associated with its substrate after the cleavage and cleaves the adjacent phosphodiester bonds. With the stronger binding affinity to DNA, one subunit of the dimeric state tends to be more effective than the monomer which dissociates from the DNA after cleavage. When the cleavage is rate limiting, the Michaelis−Menten constant K_m is approximately related to the association constant of the enzyme and the substrate. In such a situation, at least in the perspective of the binding process, from the electrostatic calculations, we find the dimer is more favorably associated with the DNA than the monomer. The cleavage chemistry controls the entire reaction, and in the experiment, the advantage of the dimeric state is not obvious as observed.

Water Dynamics in the Protein−DNA Interface. The process of the recognition and binding not only involves two partners but also involves water, ions, and other solvent. Water molecules are often observed in the protein−DNA interface. They may act as a buffer to reduce the electrostatic repulsion between DNA and protein, a packing element in recognition, a hydrogen bonding linker, and a contributor to the stability and specificity of DNA binding, i.e., *trp* repressor and restriction enzyme BamH1.[48−50] In both complex systems of SMnase, the interfacial region is highly hydrated with an average of 27 hydration sites in the monomer (Figure 7A) and 31 sites in the dimer (Figure 7B), respectively. These hydration sites were only considered where water contacts or mediates the protein and DNA simultaneously.

Such a wet interface is common for protein−DNA interfaces, especially for less specific complexes. About 65% of the interfacial hydration sites in the monomer−DNA interface and 70% in the dimer−DNA interface have residence times longer than 1.0 ps, the value for bulk water. In the monomer−DNA interface, relatively ordered water mainly mediates Asp86 and Cyt26 with residence times of hundreds of picoseconds. That means water molecules act more to screen the electrostatic region between the monomer and DNA. However, in the dimer−DNA interface, water with similar residence times

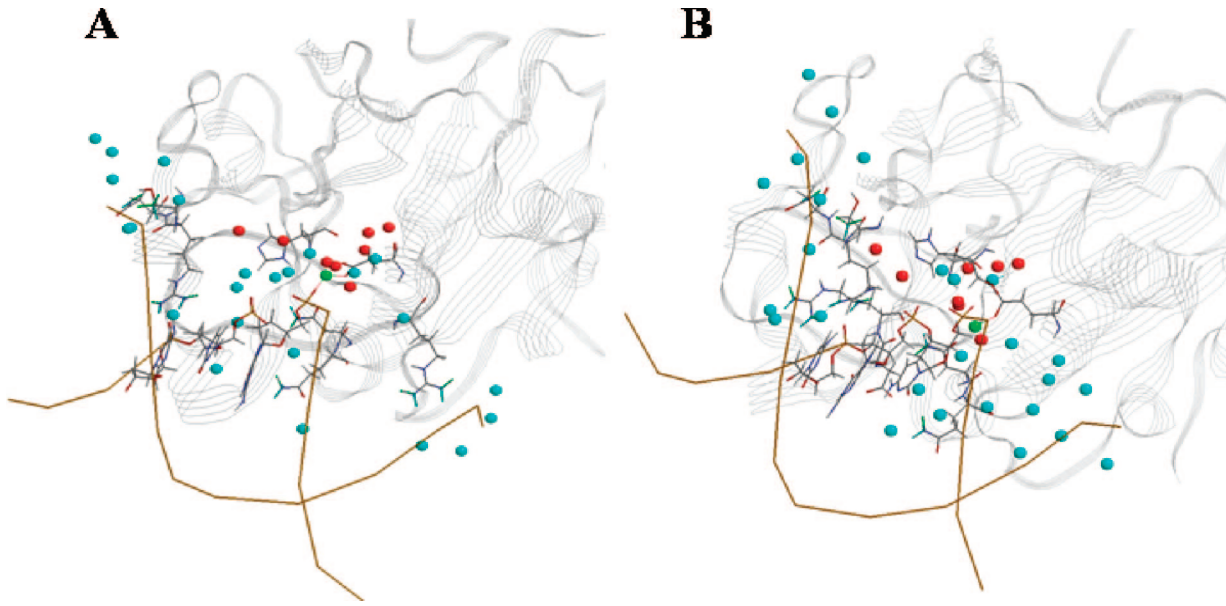

Figure 7. Hydration sites residing in the protein−DNA interface, shown in cyan spheres: (A) monomer−DNA complex; (B) dimer−DNA complex. Mg^{2+}, green sphere. Some hydration sites at the active sites are shown in red spheres.

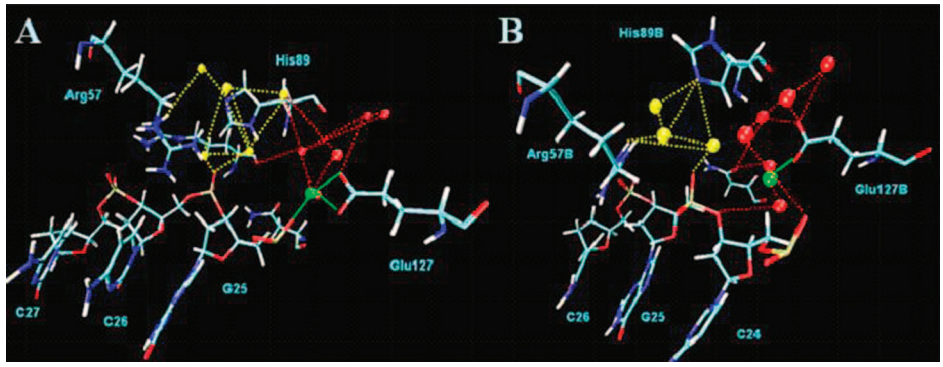

Figure 8. Water clusters at the active site: (A) monomer−DNA complex; (B) dimer−DNA complex. Mg^{2+}, green sphere. Cluster 1, "stabilizing cluster", is in red, and cluster 2, "working cluster", is in yellow. H-bond interactions are shown in dashed lines.

mainly mediates the backbone oxygen of Arg87B and Gua25 and the side chain of Arg57B and Cyt26. This indicates that in the dimer system water acts more as a glue to provide the structural adaptability with the protein and DNA.

In addition to the water residence time, the stretching parameter of the H-bond relaxations between water and water, $\beta_{HB\text{-}WW}$, is about the same in both regions with the value averaged at 0.77 ± 0.01. The H-bond lifetime of water−water, $\tau_{HB\text{-}WW}$, is about 1.03 ± 0.03 ps in the monomer complex and 0.71 ± 0.01 ps in the dimer complex, respectively. That the water−water H-bond lifetime in the dimer−DNA interface appears slightly shorter than that in the monomer−DNA interface might indicate that water in the dimer−DNA interface is less ordered and may better help facilitate DNA binding to the dimer.

Water Dynamics at the Active Site. After analyzing site−site and site−protein interactions around the active site, two water clusters were identified and distinguished according to their positions (Figure 8A for the monomer and Figure 8B for the dimer complex).The water cluster colored in red is located in the deep cleft of the active site and mainly interacts with Glu127, His89, and Mg^{2+}. The stretched beta value from the occupational relaxation, β_{res}, was estimated to be 0.67 ± 0.01 in the monomer and 0.79 ± 0.01 in the dimer complex system, respectively. Both values are smaller than 0.96 evaluated from the bulk, and β_{res} is lower in the monomer than that in the subunit B of the dimer. Such differences clearly demonstrate that water in this area in the subunit B of the dimer is less affected by both the protein and DNA, which is the same phenomenon observed in the protein systems.[20]

For the dynamics of H-bonds of water in this area, little system-dependent difference was found. The lifetime, $\tau_{HB\text{-}WW}$, was estimated to be 1.64 ± 0.02 ps in the monomer and 1.53 ± 0.07 ps in the subunit B of the dimer, respectively. In addition, $\beta_{HB\text{-}WW}$ was calculated to be 0.80 ± 0.01 in the monomer and 0.81 ± 0.02 in the dimer B. As a result, we propose the role of this water cluster is to help stabilize Mg^{2+} and below it is referred to as the "stabilizing cluster".

Another water cluster in yellow in Figure 8 is located around His89, Arg57, and the DNA phosphate group. Because of participation of His89 and Arg57 in the cleavage of DNA described by experiments, this cluster is defined as the "working cluster". β_{res}, 0.70 ± 0.01, from occupational decay in the monomer is lower than that, 0.83 ± 0.01, in the dimer complex. This is the same trend as in the stabilizing region. Although $\beta_{HB\text{-}WW}$ is similar in the monomer (0.76 ± 0.01) and in the subunit B of the dimer (0.78 ± 0.01), the lifetime, $\tau_{HB\text{-}WW}$, is 1.32 ± 0.02 ps higher than that of 0.84 ± 0.03 ps in the dimer complex, which indicates that water might have relatively stronger interactions among each other in the working region of the monomer complex and/or interact with water in the stabilizing region as well. We verified that interactions between

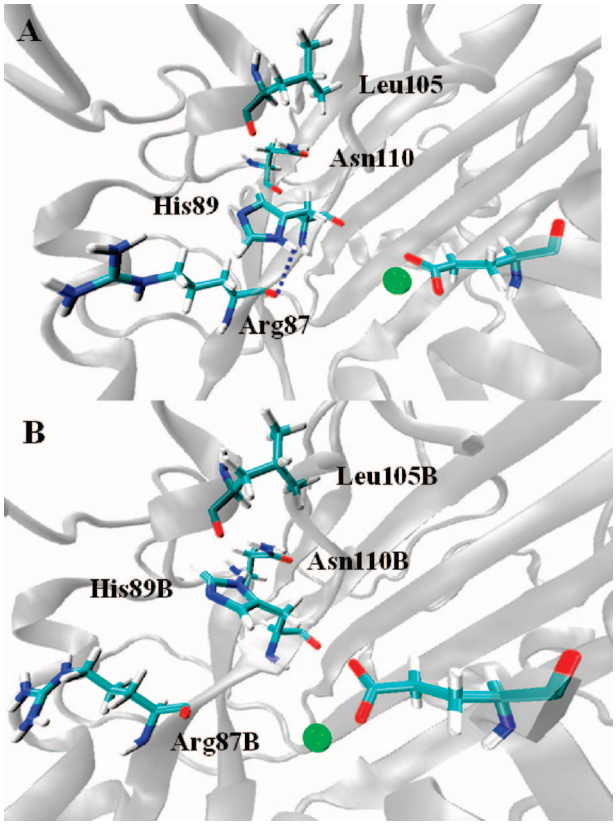

Figure 9. Interactions between His89 and other residues nearby: (A) monomer−DNA complex; (B) dimer−DNA complex.

the working cluster and the stabilizing one in the monomer system have a frequency of more than 25% but little in the dimer system.

In addition to the H-bond lifetime of water, the lifetimes of hydrogen bonds between water and protein were also analyzed. Particularly, for NE2 of His89, $\tau_{HB\text{-}WP}$ was estimated to be 3.34 ± 0.01 ps in the monomer complex and only 0.97 ± 0.02 ps in the dimer complex. Thus, water in the working region is more active in the subunit B of the dimer−DNA than in the monomer−DNA. This difference in water distribution and dynamics in the working region of the monomer and dimer complexes might be caused by the flexibilities of the side chains of key residues in the protein, such as His89 and Arg57.

Analysis of the interactions between His89 and other residues nearby showed that, in the monomer−DNA complex, during the first two 2 ns time blocks, ND1 of His89 is directly hydrogen bonded with O of Arg87 with a frequency of about 0.13. In the following 2 ns time block, rare interactions happen. In the last 2 ns time block, ND1 is hydrogen bonded to O from Leu105 with 0.12 frequency. However, in the dimer−DNA complex, ND1 of His89B interacts with ND1 of Asn110B with about the same frequency of 0.13 in all time blocks. It is noteworthy that Arg87 and Leu105/Asn110 are located on opposite sides of His89, shown in Figure 9A (monomer−DNA) and B (dimer−DNA). Thus, it is evident that the imidazole ring of His89 in the monomer−DNA complex rotates during the simulation. Such rotation can also be observed in the monomer system in the absence of DNA molecule. Therefore, given the time scale of the simulation, the flexibility of His89 resulting from dimerization might influence the dynamics of water which consequently affects the catalytic process of the enzyme.

Mechanism of the Cleavage of DNA. Although only the protein−substrate complex in binding was simulated in this

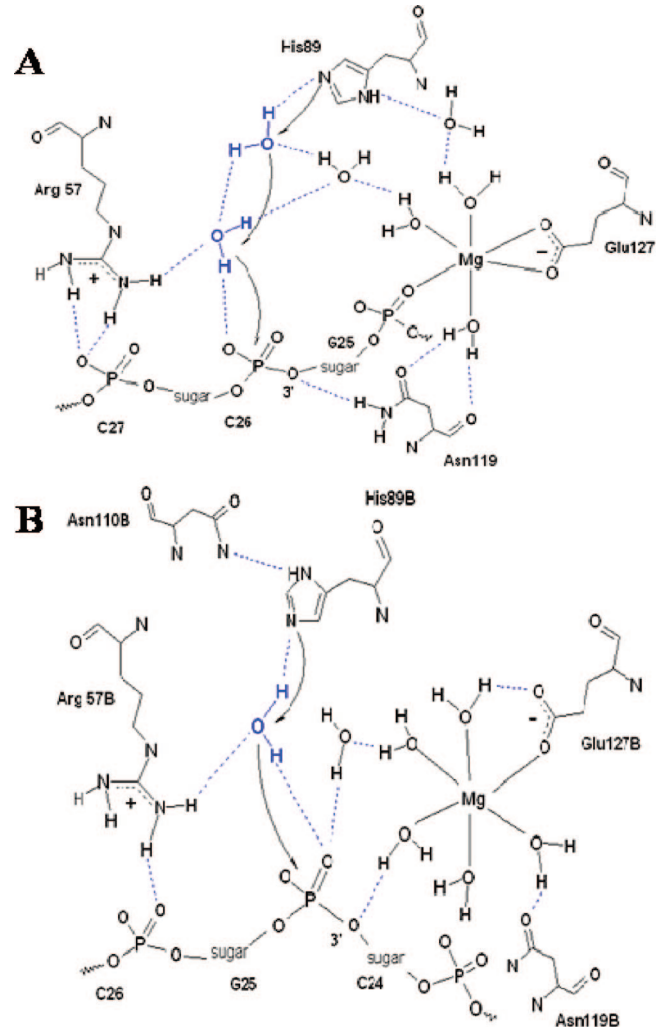

Figure 10. Proposed cleaving mechanism of SMnase: (A) monomer; (B) dimer.

work, the results above enable us to rationalize the likely mechanism of the cleavage of DNA via the resulting average structures. Generally, the complementary electrostatic potentials from protein and DNA and water residing in the protein−DNA interface facilitate DNA recognition and binding to the enzyme. However, dimerization leads to different contacts between DNA and protein residues, especially to Mg^{2+}. For the dimer form of the enzyme (Figure 10B), Asn119 loses its contact with Mg^{2+} to Glu127. Ligand waters remained constant. 3′-O of Cyt24, which is in the target scissile phosphodiester bond, binds to Mg^{2+} via a ligand water molecule. His89 plays the role of a general base to activate water molecules for a nucleophilic attack on the phosphorus atom of Gua25. The phosphoanion transition state would be stabilized by water and the Mg^{2+} water cluster.[13,14] After the cleavage of the scissile phosphodiester bond, the 5′-leaving group is in position to be stabilized by Arg57. The protonation of the 3′-leaving group is then able to occur at the expense of an Mg^{2+} bound water molecule.

However, in the monomer (Figure 10A), several differences are found. First, one nonbridging oxygen atom of Gua25 from DNA binds directly to Mg^{2+} in an inner-sphere pathway. Second, because of the flexibility of His89 and Arg57, more water molecules are involved in the working region, which seems to play multiple roles in the catalytic process. Water from that region would then be stabilizing His89 and Arg57, activated by His89, attacking the phosphorus atom, as well as stabilizing

the transition state and the 5′-leaving group. Finally, although ND2 of Asn119 interacts with 3′-O weakly in the simulation, it is considered a potential general acid candidate to protonate the 3′-leaving group.

One of the more remarkable aspects of our protein−DNA complex simulations is the finding that Asn119 does not remain chelated at all times to Mg^{2+} and further that Glu127 directly coordinates this divalent cation. These results display an equilibrium between structures, one of which is the published protein crystal structure,[14] but they may be relevant if this enzyme has plasticity in its active site configuration. We note that the simulations are based on the models built on a highly sequence-specific endonuclease I-Ppol. Thus, different sequences for the protein and nucleic acid may shift the possible structures. Furthermore, our simulations of the proteins per se[20] show that the active site Mg^{2+} configuration is consistent with the experiments, as do the short simulations of the models which are built on Vvn, a sugar-nonspecific endonuclease. Even though different active site configurations are formed in the models built on I-Ppol and Vvn, simulations all give the inner-sphere binding mode in the monomer and the outer-sphere one in the dimer. The DNA binding mode is considered to be the main cause of the different mechanisms proposed by us and others. Given the findings in our simulation, it is possible to speculate how an alternate mechanism from that previously proposed might be constructed. Of course, choosing definitively between this mechanistic picture and others will require further study.

Conclusions

The catalytic process of an enzyme generally involves recognition, association, transition-state stabilization, cleavage of the substrate, and dissociation of the product. As for the SMnase homodimer, steady-state kinetics demonstrated that two subunits can function independently of each other.[17] In addition, the gross activity of a series of monomer variants and the dimer are averaged to be the same, although SMnase attacks natural DNA in different sites with different rates.[11,17] Under the condition of low enzyme and polynucleotide concentration, likely to be in the natural habitat of the bacterium, the course of the reaction is different. The dimer form cleaves macromolecular nucleic acids processively, while the monomer works distributively.[18]

We found in our previous work on the protein systems[20] that the monomer and two subunits of the dimer differ in flexibility/dynamics of residues and water locally in the active site. In this work, we considered the effect of dimerization of SMnase simulation on model-built complexes of DNA with the monomer and dimer by molecular dynamics. By calculating the electrostatic binding energy of a 16-base-pair DNA duplex with the proteins and analyzing the hydration pattern around the systems, we found the advantage enzyme has in being a dimer in the process of association and cleavage. Specifically, dimerization leads to the rearrangement of primary contacts of DNA from the monomer to the dimer due to changes in the electrostatic field. This results in the binding pathway of DNA with the hydrated Mg^{2+} changing from an inner-sphere coordination in the monomer to an outer-sphere one in the dimer. Our results imply the outer-sphere binding pathway might be energetically favorable. Electrostatic calculations indicate that the dimer form has a more favorable association with DNA. In addition, water is observed to be more mobile in the working region of the dimer than in the monomer. Since the catalytic process is water-assisted, this leads to a more effective dimer to cleave DNA.

Acknowledgment. The authors thank Drs. Gillian Lynch and Clem Ka-yui Wong for discussions. The authors also thank Dr. Brian Beck for his support in building an earlier model on I-Ppol. This work was partially supported by grants from the NIH and the Robert A. Welch Foundation. This research was performed using the Molecular Science Computing facility (MSCF) in the William R. Wiley Environmental Molecular Sciences laboratory, sponsored by the U.S. Department of Energy's office of Biological and Environmental Research and located at the Pacific Northwest National laboratory. Structure figures were prepared with VMD.[57]

References and Notes

(1) Rangarajan, E. S.; Shankar, V. Sugar non-specific endonucleases. *FEMS Microbiol. Rev.* **2001**, *25*, 583–613.

(2) Arnone, A.; Bier, C. J.; Cotton, F. A.; Day, V. W.; Hazen, E. E.; Richardson, D. C.; Yonath, A.; Richardson, J. S. A high resolution structure of an inhibitor complex of the extracellular nuclease of Staphylococcus aureus. I. Experimental procedures and chain tracing. *J. Biol. Chem.* **1971**, *246*, 2302–2316.

(3) Miller, M. D.; Tanner, J.; Alpaugh, M.; Benedik, M. J.; Krause, K. L. 2.1 Angstrom structure of Serratia endonuclease suggests a mechanism for binding to double-stranded DNA. *Nat. Struct. Biol.* **1994**, *1*, 461–468.

(4) Shlyapnikov, S. V.; Lunin, V. V.; Perbandt, M.; Polyakov, K. M.; Lunin, V. Y.; Levdikov, V. M.; Betzel, C.; Mikhailov, A. M. Atomic structure of the Serratia marcescens endonuclease at 1.1 A resolution and the enzyme reaction mechanism. *Acta Crystallogr.* **2000**, *D56*, 567–572.

(5) Volbeda, A.; Lahm, A.; Sakiyama, F.; Suck, D. Crystal structure of Penicillium citrinum P1 nuclease at 2.8 Angstrom resolution. *EMBO J.* **1991**, *10*, 1607–1618.

(6) Li, C. L.; Hor, L.-I.; Chang, Z.-F.; Tsai, L.-C.; Yang, W.-Z.; Yuan, H. S. DNA binding and cleavage by the periplasmic nuclease Vvn: a novel structure with a known active site. *EMBO J.* **2003**, *22*, 4014–4025.

(7) Cheng, Y.-S.; Hsia, K.-C.; Doudeva, L. G.; Chak, K.-F.; Yuan, H. S. The crystal structure of the nuclease domain of ColE7 suggests a mechanism for binding to double-stranded DNA by the H-N-H endonucleases. *J. Mol. Biol.* **2002**, *324*, 227–236.

(8) Kuhlmann, U. C.; Pommer, A. J.; Moore, G. R.; James, R.; Kleanthous, C.; Hemmings, A. M. Structure of the E9 Dnase domain in comparison with the inhibited structure of the E9 Dnase/Im9 complex. Manuscript to be published.

(9) Hsia, K.-C.; Chak, K.-F.; Liang, P.-H.; Cheng, Y.-S.; Ku, W.-Y.; Yuan, H. S. DNA binding and degradation by the HNH endonuclease ColE7. *Structure* **2004**, *12*, 205–214.

(10) Mate, M. J.; Kleanthous, C. Structure-based analysis of the metal-dependent mechanism of H-N-H endonucleases. *J. Biol. Chem.* **2004**, *279*, 34763–34769.

(11) Meiss, G.; Friedhoff, P.; Hahn, M.; Gimadutdinow, O.; Pingoud, A. Sequence preferences in cleavage of dsDNA and ssDNA by extracellular Serratia marcescens endonuclease. *Biochemistry* **1995**, *34*, 11979–11988.

(12) Meiss, G.; Gast, F.-U.; Pingoud, A. M. The DNA/RNA non-specific Serratia nuclease prefers double-stranded A-form nucleic acids as substrates. *J. Mol. Biol.* **1999**, *288*, 377–390.

(13) Friedhoff, P.; Kolmes, B.; Gimadutdinow, O.; Wende, W.; Krause, K. L.; Pingoud, A. *Analysis of the mechanism of the Serratia nuclease using site-directed mutagenesis. Nucleic Acids Res.* **1996**, *24*, 2632–2639.

(14) Miller, M. D.; Cai, J.; Krause, K. L. The active site of Serratia endonuclease contains a conserved magnesium-water cluster. *J. Mol. Biol.* **1999**, *288*, 975–987.

(15) Kuhlmanna, U. C.; Moore, G. R.; James, R.; Kleanthous, C.; Hemmings, A. M. Structural parsimony in endonuclease active sites: should the number of homing endonuclease families be redefined? *FEBS Lett.* **1999**, *463*, 1–2.

(16) Friedhoff, P.; Franke, I.; Meiss, G.; Wende, W.; Krause, K. L.; Pingoud, A. A similar active site for non-specific and specific endonucleases. *Nat. Struct. Biol.* **1999**, *6*, 112–113.

(17) Franke, I.; Meiss, G.; Belcher, D.; Gimadutdinow, O.; Urbanke, C.; Pingoud, A. Genetic engineering, production and characterisation of monomeric variants of the dimeric. *Serratia marcescens endonuclease. FEBS Lett.* **1998**, *425*, 517–522.

(18) Franke, I.; Meiss, G.; Pingoud, A. On the advantage of being a dimer, a case study using the dimeric Serratia nuclease and the monomeric nuclease from Anabaena sp. Strain PCC 7120. *J. Biol. Chem.* **1999**, *274*, 825–832.

(19) Chen, C.; Beck, B. W.; Krause, K. L.; Pettitt, B. M. Solvent participation in Serratia marcescens endonuclease complexes. *Proteins: Struct., Funct., Bioinf.* **2006**, *62*, 982–995.

(20) Chen, C.; Beck, B. W.; Krause, K. L.; Pettitt, B. M. The effects of dimerization of Serratia marcescens endonuclease on water dynamics. *Biopolymers* **2007**, *85*, 241–252.

(21) Jen-Jacobson, L. Protein-DNA recognition complexes: conservation of structure and binding energy in the transition state. *Biopolymers* **1997**, *44*, 153–180.

(22) Oda, M.; Nakamura, H. Thermodynamic and kinetic analyses for understanding sequence-specific DNA recognition. *Genes Cells* **2000**, *5*, 319–326.

(23) Brooks, B. R.; Bruccoleri, R. E.; Olafson, B. D.; States, D. J.; Swanminathan, S.; Karplus, M. CHARMM: a program for macromolecular energy, minimization, and dynamics calculations. *J. Comput. Chem.* **1983**, *4*, 187–217.

(24) Smith, P. E.; Holder, M. E.; Dang, L. X.; Feig, M.; Pettitt, B. M. *ESP*; University of Houston: Houston, TX, 1996.

(25) MacKerell, A. D.; Bashford, D.; Bellott, R. L.; Dunbrack, R. L.; Evanseck, J.; Field, M. J.; Fischer, S.; Gao, J.; Guo, H.; Ha, S.; Joseph, D.; Kuchnir, L.; Kuczera, K.; Lau, F. T. K.; Mattos, C.; Michnik, S.; Ngo, T.; Nguyen, D. T.; Prodhom, B.; Reiher, W. E., III; Roux, B.; Schlenkrich, M.; Smith, J.; Stote, R.; Straub, J.; Watanabe, M.; Wiorkiewicz-Kuczera, J.; Yin, D.; Karplus, M. All-atom empirical potential for molecular modeling and dynamics studies of proteins. *J. Phys. Chem. B* **1998**, *102*, 3586–3616.

(26) Foloppe, N.; Mackerell, A. D. All-atom empirical force field for nucleic acids: I. Parameter optimization based on small molecule and condensed phase macromolecular target data. *J. Comput. Chem.* **2002**, *21*, 86–104.

(27) de Leeuw, S. W.; Perram, J. W.; Smith, E. R. Ewald summations and dielectric constants. *Proc. R. Soc. London* **1980**, *A373*, 27–56.

(28) Sharp, K. A.; Honig, B. Calculation total electrostatic energies with nonlinear Possion-Boltzmann equation. *J. Phys. Chem.* **1990**, *94*, 7684–7692.

(29) Misra, V. K.; Sharp, K. A.; Friedman, R. A.; Honig, B. Salt-effects on ligand-DNA: binding minor groove binding antibiotics. *J. Mol. Biol.* **1994**, *23*, 8–263.

(30) Baker, N. A.; Sept, D.; Joseph, S.; Holst, M. J.; McCammon, J. A. Electrostatics of nanosystems: application to microtubules and the ribosome. *Proc. Natl. Acad. Sci. U.S.A.* **2001**, *98*, 10037–10041.

(31) Nina, M.; Im, W.; Roux, B. Optimized atomic radii for protein continuum electrostatic solvation forces. *Biophys Chem.* **1999**, *78*, 89–96.

(32) Makarov, V. A.; Andrews, B. K.; Smith, P. E.; Pettitt, B. M. Residence times of water molecules in the hydration sites of myoglobin. *Biophys J.* **2000**, *79*, 2966–2974.

(33) Bizzarri, A. R.; Cannistraro, S. Molecular dynamics of water at the protein-solvent interface. *J. Phys. Chem. B* **2002**, *106*, 6617–6633.

(34) Shamblin, S.; Hancock, B. C.; Dupuis, Y.; Pikal, M. J. Interpretation of relaxation time constants for amorphous pharmaceutical systems. *J. Pharm. Sci.* **2000**, *89*, 417–427.

(35) Yoshioka, S.; Tajimar, S.; Aso, Y.; Kojima, S. Inactivation and aggregation of β-galactosidase in lyophilized formulation described by Kohlrausch-Williams-Watts stretched exponential function. *Pharm. Res.* **2003**, *20*, 1655–1660.

(36) Paul, S.; Chandra, A. Hydrogen dynamics at vapor-water and metal-water interface. *Chem. Phys. Lett.* **2004**, *386*, 218–224.

(37) Bandyopadhyay, S.; Chakraborty, S.; Bagchi, B. Secondary structure sensitivity of hydrogen bond lifetime dynamics in the protein hydration layer. *J. Am. Chem. Soc.* **2005**, *127*, 16660–16667.

(38) Cowan, J. A. Metal activiation of enzymes in nucleic acid biochemistry. *Chem. Rev.* **1998**, *98*, 1067–1087.

(39) Adrian-Scotto, M.; Vasileva, D.; Mallet, G.; Vasilescu, D. About hydration of Mg 2+: a quantum DFT study. Internet electron. *J. Mol. Des.* **2004**, *4*, 400–411.

(40) Markham, G. D.; Glusker, J. P.; Bock, C. L.; Trachtman, M.; Bock, C. W. Hydration energies of divalent beryllium and magnesium Ions: An ab initio molecular orbital study. *J. Phys. Chem.* **1996**, *100*, 3488–3497.

(41) Black, C. B.; Cowan, J. A. Inert chromium and cobalt complexes as probes of magesium-dependent enzymes: Evaluation of the mechanistic role of the essential metal cofactor in Escherichia coli exonuclease III. *Eur. J. Biochem.* **1997**, *243*, 684–689.

(42) Petrov, A. S.; Lamm, G.; Pack, G. R. Water-mediated magnesium-guanine interactions. *J. Phys. Chem. B* **2002**, *106*, 3294–3300.

(43) Misra, V. K.; Hecht, J. L.; Yang, A. S.; Honig, B. Electrostatic contributions to the binding free energy of the ëcI repressor to DNA. *Biophys. J.* **1998**, *75*, 2262–2273.

(44) Antosiewicz, J.; McCammon, J. A.; Glison, M. K. Prediction of pH-dependent properties of proteins. *J. Mol. Biol.* **1994**, *238*, 415–436.

(45) Antosiewicz, J.; Miller, M. D.; Krause, K. L.; McCammon, J. A. Simulation of electrostatic and hydrodynamic properties of Serratia endo-nuclease. *Biopolymers* **1997**, *44*, 443–450.

(46) Record, M. T.; Lohman, T. M.; deHaseth, P. Ion effects on ligand-nucleic acid interactions. *J. Mol. Biol.* **1976**, *107*, 145–158.

(47) Olmsted, M. V.; Bond, J. P.; Anderson, C. F.; Record, M. T. Grand canonical Monte Carlo molecular and thermodynamic predictions of ion effects on binding of an oligocation (L^{8+}) to the center of DNA oligomers. *Biophys. J.* **1995**, *68*, 634–647.

(48) Jayaram, B.; Janin, T. The role of water in protein-DNA recognition. *Annu. Rev. Biophys. Biomol. Struct.* **2004**, *33*, 343–361.

(49) Joachimiak, A.; Haran, T. E.; Sigler, P. B. Mutagensis supports water mediated recognition in the trp repressor-operator system. *EMBO J.* **1994**, *13*, 367–372.

(50) Newman, M.; Strzelecka, T.; dorner, L.; Schildkraut, I.; Aggarwal, A. K. Structure of BamH1 endonuclease bound to DNA: partial folding and unfolding on DNA binding. *Science* **1995**, *269*, 656–663.

(51) Dong, F.; Vijayakumar, M.; Zhou, H. X. Comparison of calculation and experiment implications significant electrostatic contributions to the binding stability of barnase and barstar. *Biophys. J.* **2003**, *85*, 49–60.

(52) Smith, P. E.; Brunne, R. M.; Mark, A. E.; van Gunsteren, W. F. Dielectric properties of trypsin inhibitor and lysozyme calculated from Molecular Dynamics simulations. *J. Phys. Chem.* **1993**, *97*, 2009–2014.

(53) Pitera, J. W.; Falta, M.; van Gunsteren, W. F. Dielectric properties of proteins from simulation: the effects of solvent, ligands, pH, and temperature. *Biophys. J.* **2001**, *80*, 2546–2555.

(54) Yang, L.; Weerasinghe, S.; Smith, P. E.; Pettitt, B. M. Dielectric response of triplex NA in ionic solution from simulations. *Biophys. J.* **1995**, *69*, 1519–1527.

(55) Reddy, M. R.; Berkowitz, M. Dielectric constant of SPC/E water. *Chem. Phys. Lett.* **1989**, *155*, 173–176.

(56) Frank, F., Ed. *Water—A comprehensive treatise*; Plenum: New York, 1973; Vols. *1* and *3*.

(57) Humphrey, W.; Dalke, A.; Schulten, K. VMD: visual molecular dynamics. *J. Mol. Graphics* **1996**, *14*, 33–38.

JP8057838